Front. Phys. 10, 104204 (2015)
DOI 10.1007/s11467-014-0450-0

RESEARCH ARTICLE

Characteristics of indirect laser-induced plasma from a thin film of oil on a metallic substrate

Jun-Shan Xiu (修俊山)[1,†], **Xue-Shi Bai** (白雪石)[2], **Vincent Motto-Ros**[2], **Jin Yu** (俞进)[2]

[1] *Department of Sciences, Shandong University of Technology, Zibo 255049, China*

[2] *Institut Lumière Matière, UMR5306 Université Lyon 1-CNRS, Université de Lyon, 69622 Villeurbanne Cedex, France*

Corresponding author. E-mail: †*xiujunshan@126.com*

Received June 19, 2014; accepted September 13, 2014

Optical emissions from the major and trace elements embodied in a transparent gel prepared from cooking oil were detected after the gel was spread in a thin film on a metallic substrate. Such emissions are due to the indirect breakdown of the coating layer. The generated plasma, a mixture of substances from the substrate, the layer, and the ambient gas, was characterized using emission spectroscopy. The characteristics of the plasma formed on the metal with and without the coating layer were investigated. The results showed that Al emission induced from the aluminum substrates coated with oil films extends away from the target surface to ablate the oil film. This finally formed a bifurcating circulation of aluminum vapor against a spherical confinement wall in the front of the plume, which differed from the evolution of the plasma induced from the uncoated aluminum target. The strongest emissions of elements from the oil films can be observed at 2 mm above the target after a detection delay of 1.0 μs. A high temperature zone has been observed in the plasma after the delay of 1.0 μs for the plasma induced from the coated metal. This higher temperature determined in the plasma allows the consideration of the sensitive detection of trace elements in liquids, gels, biological samples, or thin films.

Keywords indirect laser-induced plasma, thin layer, aluminum substrate, higher temperature

PACS numbers 42.62. Fi, 52.25.Kn, 52.25.Os, 52.70.Kz, 52.90.+z

1 Introduction

Elementary analysis of viscous liquids such as oils or gels using laser-induced breakdown spectroscopy can provide important information in the assessment of the performance and quality of a sample. For example, trace elements in cooking oil can be used to decide whether a particular cooking oil is eligible for use in cooking [1]; changes in the basic elements in a lubricating oil can be used to assess the performance of that oil [2]; and the thickness of a thin film can be determined by the detection of the elements in thin film [3]. Although several conventional methods, such as ICP-MS, ICP-OES and AAS, can provide sensitive and precise results, detection using these methods is mainly completed in laboratories and not appropriate for field measurements. Therefore, it is desirable to introduce a real-time rapid analysis technique to detect the elements in gel samples.

Laser induced breakdown spectroscopy (LIBS) technology is a rapid, online, sensitive and multi-element analysis method that has received more and more attention in recent decades [4–7]. It has been extensively used for a wide range of scientific and industrial applications with varying degrees of success [8–12]. However, due to some inherent drawbacks such as splashing, absorption, and fast quenching of plasmas in the liquid samples [5], the LIBS signal produced in gel samples shows more noise and less stability compared with solid samples, which results in lower detection sensitivity and shorter lifetime of plasma.

A number of investigations that improve the LIBS signals of liquid samples in the form of static surfaces [13, 14], jets [15, 16], liquids on different substrates [17–21] and aerosols [22] have been reported. Moreover, for gel samples, such as lubricating oils, several methods used for liquid samples have achieved many good results, such as jets [23], static surfaces [13, 23], and paper substrates [24]. Amongst these approaches, using a paper substrate was the preferred method for obtaining the optimal LIBS

© Higher Education Press and Springer-Verlag Berlin Heidelberg 2015

signal because of its ability to prevent splashing, which means that the plasma-collecting lens can be located closer to the ablation point. Recently a new substrate, made of a metallic alloy, was used successfully to detect manganese in liquid samples [25]. It showed that 10-μL microdroplets of manganese solution were placed on an aluminum substrate and given 15 min to dry, on the surface of which a hot and dense plasma was produced which engulfed the droplet and enhanced the LIBS signal.

The objective of this work is to investigate whether it is possible to use a metallic aluminum alloy substrate for LIBS analysis of gel samples. It will explain the enhancement of LIBS signals through the evolution of plasma induced from the aluminum substrate. In this work, a cooking oil sample will be smeared and distributed evenly on the surface of the aluminum alloy to form one thin layer of oil film. The plasma is induced from the aluminum substrate both with and without the thin oil film in an argon ambient gas at a pressure of one atmosphere. The plasma characteristics are investigated by time- and space-resolved spectroscopy and the evolution of the plasma will be observed using a plasma imaging technique.

2 Experimental setup

The experimental setup used is presented in Fig. 1. The fundamental output of a Q-switched Nd:YAG laser (Quantel Brilliant) with a 10-ns laser pulse duration, operated at 10 Hz was delivered to the surface of a certified aluminum alloy (Al 89.5%, Si 8.39%, Fe 0.999%, and some trace elements). The laser pulse energy was fixed at 85 mJ. The laser beam was reflected by a high reflection mirror (M1) and passed through an ensemble consisting of a half-wave plate (HWP) and a Glan prism (GP). Such an ensemble allows for fine adjustments in the laser energy so that a constant laser energy could be delivered to the surface of the target. A mechanical beam shutter (BSH) controlled the delivery of the laser pulse, and a beam splitter sent 4% of a pulse to a photodiode (PD). A synchronization signal was thus generated and used to trigger two detection systems simultaneously. The laser pulse was focused on the surface of a metallic aluminum alloy by a lens of 50 mm focal length (L1). In order to avoid a direct breakdown in the ambient gas, the focus point of the beams was set under the surface with a shift of about 1 mm. The aluminum alloy was mounted on a motorized micrometric stage with X-Y-Z displacement ability in order to provide a fresh surface for each burst of laser shot. The distance between the focus lens (L1) and the target surface was kept constant during the measurements by a monitoring system that consisted of a laser pointer with the beam delivered obliquely onto the target surface and a video camera installed above the mirror (M2). A pair of tubes was placed above the target in order to deliver a stream of argon gas with a fixed flow of 8 L/min, which ensured that the plasma would expand into pure argon, ambient at a pressure of 1 atm. The emission plasma was detected simultaneously using 2 two-lens systems in a 4-f configuration (L2, L3 and L4, L5 in Fig. 1). The combination of the two lenses L2 and L3 with focal lengths of 7.5 cm and 5 cm, respectively, was used in order to form a reduced image of the induced plasma. An optical fiber of 50-μm core diameter was positioned in the image plane in order to capture a part of the emission from the plasma with spatial resolution. In this paper, axial profiles will be presented, which were obtained by translating the fiber systematically along the incident axis of the laser (z axis) at the middle transversal position of the image of the plasma. Such a detection system allowed a spatial resolution of 75 μm for local detection of the plasma emission. The output of the fiber was connected to the entrance of an Echelle spectrometer, which was in turn connected to an intensified charge-coupled device (ICCD) camera (Mechelle 5000 and iStar DH734-18F-05 made by Andor Technology, England). The combination of the two lenses L4 and L5 with focal lengths of 6 cm and 20 cm, respectively, were used to form a magnified image of the plasma induced. The image was directly recorded by another ICCD camera (iStar DH334T-18F-03 made by Andor Technology, England) placed at the image plane. A narrowband filter (F in Fig. 1) was inserted between the two lenses of the 4-f system in order to take an image of the plasma with the emission in the bandwidth selected by the filter. Each spectrum and image was recorded for 20 shots accumulating in 20 shots of the target all taken at different positions.

The plasma emissions were measured with spatial resolution by translating the fiber along the incident axis of the laser (z axis) at the middle transversal position of the image of the plasma. The temporal evolution of the plasma was investigated by measuring space-resolved emissions in three different detection windows (500–900 ns, 1000–1500 ns, and 2000–3000 ns) after the arrival of a laser pulse on the surface of the sample. Henceforth, we will use the notation D500, D1000, and D2000 to, respectively, denote the three detection windows. In order to directly compare the emission intensities measured at different detection time delays, the signal was divided by the gate width. This leads to a representative value of the signal for the delay interval concerned, independent of the chosen gate width. In the earliest stage of the

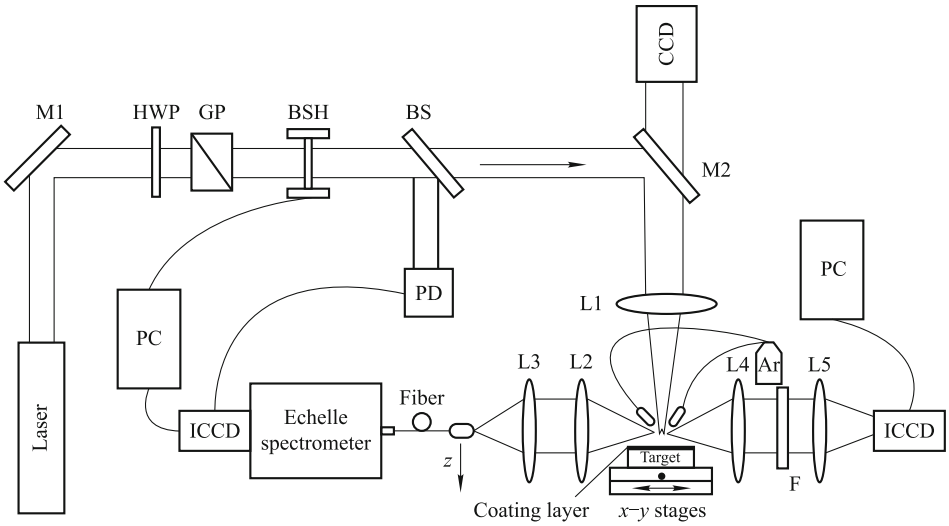

Fig. 1 Experimental setup for plasma diagnostics using two different collection configurations. M1 & M2: Mirrors, L1–L5: Lenses, HWP: Half wave plate, GP: Glan prism, BSH: Beam shutter, BS: Beam splitter, F: Filter, PC: Personal computer, PD: Photodiode, ICCD: ICCD camera.

plasma, the strong continuum prevents the observation of line emissions from different species in the plasma. The intensities measured in our experiments were integrated along the line-of-sight (y axis). By assuming a cylindrical symmetry of the plasma, the Able inversion was applied to obtain the plasma emissivity as a function of its radius. Considering the magnification of ~ 0.67 of the image system, the measurements were performed at physical distances of $z = 0.8$ and 1.6 mm, respectively, close to the target surface around the middle of the plasma.

An oil sample was prepared with a ratio of 1:1 between cooking oil and surfactant dissolving a saturated concentration of NaCl. A 5 mL oil sample was smeared and distributed evenly on the surface of the aluminum alloy to form one thin layer of oil film with a thickness ~ 15 μm, see the coating layer shown in Fig. 1. The prepared sample was left for 5 min prior to laser ablation in order for the oil layer to be stabilized on the target surface. After analysis, the target surface was cleaned (using distillated water and ethanol) and re-polished for use with a new liquid sample.

3 Results and discussion

3.1 Emission spectrum of a plasma induced on aluminum with a thin film of oil

Figure 2 shows a typical emission spectrum for a plasma induced on a metallic aluminum alloy covered by a thin layer of oil film. This spectrum is obtained using a time detection window of 1 μs and a delay time of 1 μs. The emission lines of different elements from the oil film (Na, Ca, H, C, and Cl), aluminum target (Al, Fe and Si), and ambient gas (Ar) are observed. This indicates that one laser pulse is focused on the surface of the aluminum alloy, ablating to produce a high-temperature plasma, and the covered oil film and ambient gas will be ablated indirectly. We note that the strongest emission line from the chlorine (at 837.6 nm) appears much weaker when compared to the other lines in the spectrum. For this reason, we present separately the chlorine line in the inset of Fig. 2 using an amplified scale. Emissions from the specific elements of the oil layer indicates its breakdown and vaporization and furthermore a high temperature in the plume. The emission from Cl especially provides further proof of such a high temperature through the high up-level energy of 10.4 eV of the corresponding transition [26]. For the directed detection of the oil film, the temperature is very low and the emission signal is weak as the plasma was induced in a gel sample. Therefore, this is considered to be an effective approach to sensitively detect chlorine in oil, which is very important for the discrimination between hogwash and edible oils [1].

The choice of the representative lines for different species in the plasma was guided by the consideration of a negligible self-absorption for these lines. An elementary precaution is to avoid using, if possible, the ground state as the level of the chosen transition. The selected lines should allow a complete representation of the distributions of elements evaporated from different parts of a sample such as the target, the gel layer, and the ambient gas. In our experiment, according to the criteria for line selection, the Al I (309.3 nm) evaporated from the aluminum target and the Ar I (696.5 nm) and Ar II

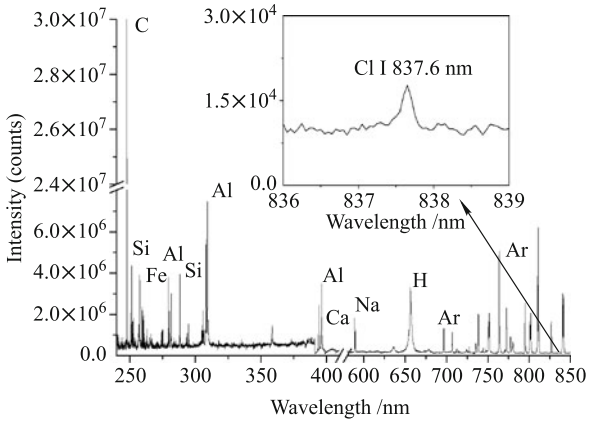

Fig. 2 Typical emission spectrum of the mixture plasmas of the substances from the metallic substrate and the oil film with the indications of the main observed elements. The insert shows the detailed spectra for the Cl element.

(480.6 nm) evaporated from the ambient gas were determined, which were the same as the selection used in Ref. [27]. The Na I (588.9 nm) and Cl I (837.6 nm) were evaporated from the oil film.

3.2 Emission intensity profiles of the elements from the target and from the thin film

3.2.1 Axial profiles

To define the evolution of a plasma induced from an aluminum substrate coated with oil film, the plasma emissions of different species are analyzed using time- and space-resolved laser-induced breakdown spectroscopy. In this work, we compare the plasma from the aluminum substrate coated with oil film with that from an uncoated aluminum substrate. Figure 3 shows the axial profiles of normalized emission intensities of different species in the plasma from two different samples with the delay times of 0.5, 1.0 and 2.0 μs. Spectra are detailed for Al I (309.3 nm) from the aluminum target (Fig. 3(a)), Ar I (696.5 nm) from the ambient gas (Fig. 3(b)), Ar II (480.6 nm) from the ambient gas (Fig. 3(c)), and Na I (588.9 nm) and Cl I (837.6 nm) from the oil film (Fig. 3(d)). In Fig. 3, the axial position represents the distance in the plasma with respective to the aluminum target surface. The origin of the axis corresponds to the surface. Significant differences can be observed for Al emission from the two different substrates in Fig. 3(a). It can be seen that Al emission from the coated aluminum substrate has a larger shift away from the target surface than that of the uncoated aluminum substrate. It is also weaker near the target surface (scarcely any signals) when comparing the uncoated aluminum substrate with the same normalized procedure. With increasing delay time, the strongest Al emission extends away from the target surface, while for the Al plasma emission from the coated aluminum substrate the extension is larger, especially between the delays of 0.5 μs and 1.0 μs. This indicates that hot Al plasma emission from coated aluminum substrates ablates the thin layer of oil film so that it is farther away from the target surface and has a larger emission zone. In Fig. 3(b), the profiles of Ar emission exhibit a similar trend for two different substrates and the strongest emissions for the Ar are in the periphery of the plasma. However, the Ar emissions from the coated aluminum substrate are weaker with delays of 1.0 μs and 2.0 μs using the same normalized procedure than those of the uncoated aluminum substrate. This suggests that hot Al plasma emission ablates simultaneously the oil film and the Ar ambient gas, causing the Ar emissions to be weaker. Figure 3(c) shows that at a short delay of 0.5 μs, Ar^+ emission from the coated sample shifts toward the target surface with respect to that from the uncoated sample. Moreover, the relative position of the emission zone of $Ar^+$from the coated sample has an obvious shift toward the target surface with respect to that of Ar, as shown in Figs. 3(b) and (c). The observed arrangement of the axial profiles of the elemental emissions from the Ar^+ and Ar in the ambient gas suggests a significant temperature gradient that goes from the middle of the plasma to its periphery. Figure 4(d) shows Na and Cl emissions from the plasma of the coated aluminum substrate. We note that at a delay of 0.5 μs, the Cl emission is disturbed by a strong background emission so it is impossible to have a representative spatial profile of its emission. At longer delays of 1.0 μs and 2.0 μs, it can be seen that the strongest Na and Cl emissions have the same position as an Ar emission away from the target surface, at about 2.0 mm for the delay of 1.0 μs. This indicates an upward displacement of the high temperature zone in the plume. Such displacement can be verified from the appearance of a zone of emission of chlorine in the front of the plume. The high excitation energy of the chlorine line (10.4 eV) provides proof of high temperature in this zone.

For the uncoated Al substrate, the Al plasma emission extends near the target surface, while for the coated Al substrate, hot Al plasma emission extends away from the target surface and ablates the thin oil film and ambient gas indirectly. The Na and Cl in the oil film are excited in the periphery of the plasma. To obtain an optimal Cl signal, the delay time should be set to be after 1.0 μs and the detection window will be 2 μs.

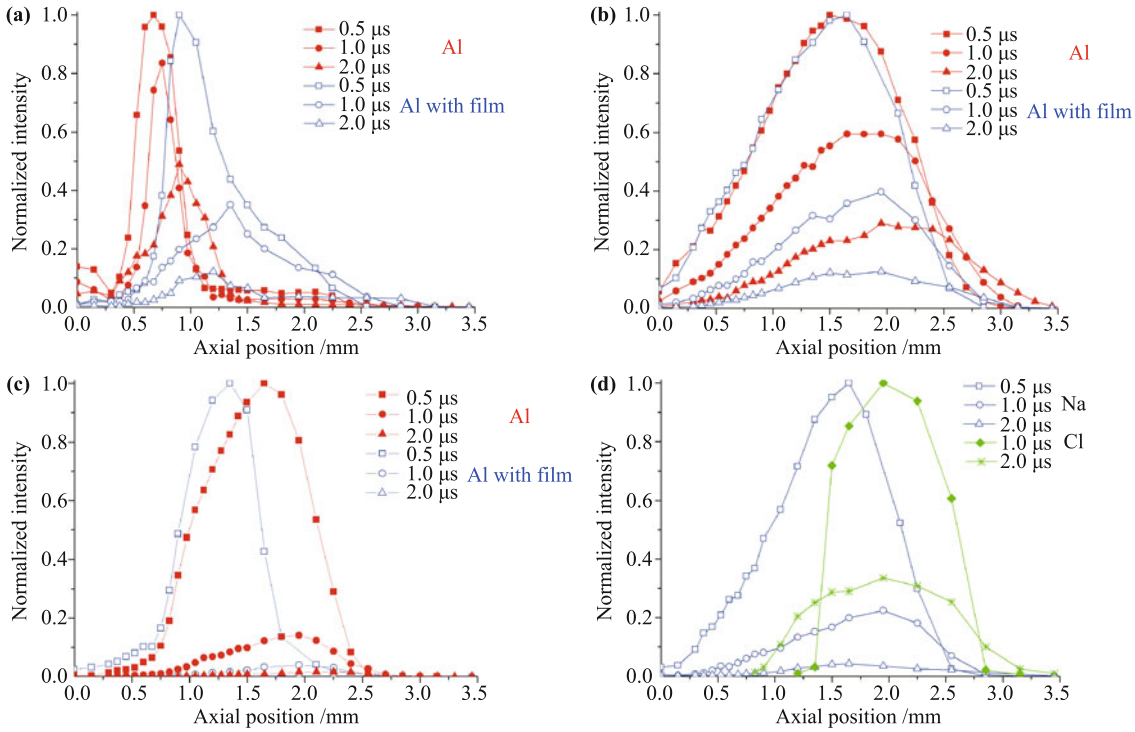

Fig. 3 Axial distribution of the elements in the plasma from aluminum substrate with and without thin layer oil film in different delay times. Different species in the plasma are **(a)** neutral aluminum evaporated from the aluminum substrate, **(b)** neutral and **(c)** ionic argon contributed by the ambient gas, and **(d)** neutral sodium and neutral chlorine ablated from the oil film. The detection windows of three delays are 400 ns, 500 ns and 1000 ns, respectively.

3.2.2 Radial profiles

In order to obtain more detailed information on the evolution of the plasma induced from the coated aluminum target, transversal profiles have been performed at two different axial distances of 0.8 and 1.5 mm, which correspond to the real distances of 1.2 and 2.25 mm from the plasma. The Abel inversion descried in Ref. [28] has been implemented to accede to the radial distributions of the plasma. Such distributions provide us with a description of the radial expansion of the plasma and allow us to confirm the representativity of line-of-sight integrated axial measurements for the plasma core. In our experiments, in order to check the symmetry of the plasma, transversal scans have been performed for both sides of the plasma with respect to its symmetrical axis. Once the symmetry is verified (allowing for the experimental noise), we average the two parts of the signal to obtain a mean radial distribution. Finally, for the presentation of the results with a more realistic representation of the plasma, we plot the other half of the distribution using symmetry. These notices have been verified in our previous work [29].

In our experiments, radial distributions of three elements evaporated from different parts of the sample are observed. Al was evaporated from the target, Ar from the ambient gas and Na from the oil film. In Fig. 4, we present the emissivities of Al I (line at 309.3 nm), Ar I (line at 696.5 nm), and Na I (line at 588.9 nm) at z= 0.8 mm and 1.5 mm. For Al, the distributions with a maximum at the middle of the plasma are observed for D500 and D1000 at z= 0.8 mm and D500 at z= 1.5 mm, which can be fitted by Gaussian functions as also observed by Sakka *et al.* [30]. However, for the profiles at z = 0.8 mm, the emissivity of Al showed a minimum in the middle of the plasma at the delay of 2000 ns, as shown in Fig. 4(a). For the profiles at z= 1.5 mm, the emissivity of Al shows similar patterns at the delays of 1000 and 2000 ns, as shown in Fig. 4(b). We obtain the result that the emissivity of Al expanded generally at a short delay of 500 ns, while as the delay increases, it exhibits a central distribution delimited at a peripheral zone where the emissivity monotonically decreases. It is the case that a part of the population seems to be transferred from the region around the central axis of the plume to its periphery regions within bifurcating flows. The closer you get to the target surface, the earlier to represent the situation, observed in Figs. 4(a) and (b). For Ar, the emissivity profiles distribute evenly around the middle of the plasma, while at the longer delay it shows a slight minimum in the central distribution and the edge of the distributions are less steep with the expansion into the

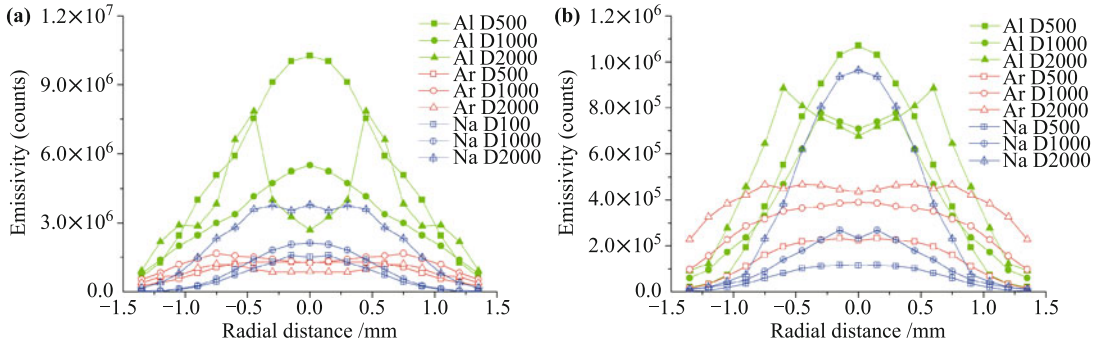

Fig. 4 Radial profiles of the emissivities of Al, Ar and Na for the three different delays at **(a)** z=0.8 mm and **(b)** z=1.5 mm.

outside of the plasma in the emission zone of argon. Such behavior is thus specific to the plasma induced with the gel layer, which is different with our previous observations in Ref. [29], in which the expansion of the plasma is induced by IR laser pulse on the surface of an aluminum target in argon ambient gas. For Na, the emissivity profiles exhibit particularly high values in the central part of the plasma, which confirms in the radial direction the strong interaction between the Al vapor and the oil film in the axial profiles. It also determines that the strongest emissions evaporated from the oil film are observed in the central axial profile. This explained why we are able, in our experiments, to observe the emission profile of the chlorine contained in the oil film, as shown in Fig. 3(d).

3.3 Behavior of the plume expansion

To confirm the evolution of the plasma induced from the coated aluminum substrate at different delay times, spectroscopic images are used to observe the process intuitively. In this work, Al emission in the plasma is imaged using a narrowband filter (with a central wavelength of 400 nm and a bandwidth of 10 nm). Figure 5 shows spectroscopic images of the neutral aluminum vapor taken at time delays of 0.5, 0.75, 1.0, 1.5, and 2.0 μs. Each image in Fig. 5 represents a real dimension of 3 × 3 mm^2. The bottom line of the picture indicates the target surface. At the short time delay of 0.5 μs, the background emission might be extremely strong, owing to which the image of the plasma cannot represent completely the Al emission. However, in this study the specific distribution of different species in the plasma have not been investigated; Al emission, including background emission, can still show the position of Al plasma with regard to the target surface and the evolution of the Al plasma as shown in Fig. 5.

At a short time delay of 0.5 μs, we can see an aluminum plume delimited in its axial propagation by a nearly spherical surface in its front (Fig. 5(a)). As delay increases, a part of the population seems to be transferred from the region around the central axis of the plume to

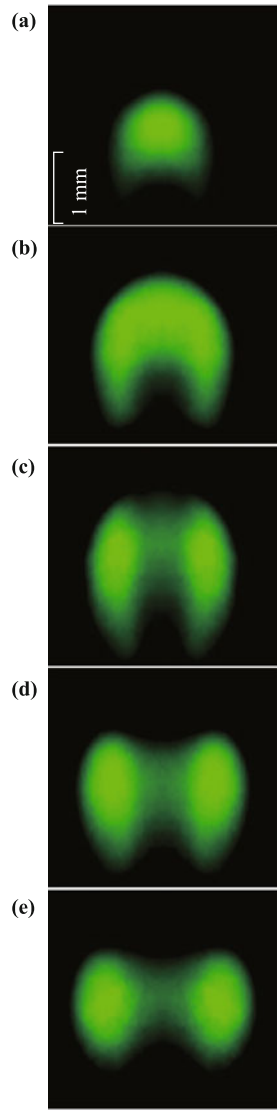

Fig. 5 Al emissivity images obtained from the aluminum substrate with (a–e) in different delay times: **(a)** 0.5 μs, **(b)** 0.75 μs, **(c)** 1.0 μs, **(d)** 1.5 μs and **(e)** 2.0 μs. The corresponding detection windows are 50 ns, 50 ns, 100 ns, 100 ns and 200 ns, respectively. The real dimension of each picture is 3 mm × 3 mm and the bottle line of each image corresponds to the target surface.

its periphery regions within bifurcating flows along the internal wall of the spherical confinement surface (Fig. 5(b)). Such bifurcating flows finally transport most of the population into the peripheral regions, leaving the region around the central axis depopulated (Fig. 5(c)). At longer delays of 1.5 and 2.0 μs, the Al emission becomes weak and maintains only its strongest part in the periphery of the plasma (Figs. 5(d) and (e)). During the bifurcating population transfer, the aluminum vapor is kept in close contact with the confining layer, which would allow its efficient heating by the aluminum vapor. Such a mechanism corresponds well with the observation of chlorine emission at delays longer than 1 μs in the front of the plume (Fig. 3(d)).

3.4 Profiles of electron density and temperature

In order to study the physical properties of the plasma and its evolution, the profiles of two important plasma parameters, the electron density and the plasma temperature, are measured in our experiment. Figure 6 shows the profiles of the electron density and the temperature measured in the plasma induced from the coated and uncoated aluminum substrate at 3 delays of 0.5, 1.0 and 2.0 μs. These parameters are deduced by the standard plasma diagnostics methods. The proper choice of elements and associated emission lines has an effect on the precision of the resulting plasma parameters. In this work, the electron density is calculated by the Stark broadening of the Ar I 696.5-nm line for the uncoated aluminum substrate in the Ar ambient gas, and the H_α 656.27 nm line for the coated aluminum substrate in the Ar ambient gas. As for the Ar ambient gas, the Ar I 696.5 nm line has been verified to be a reliable reference line for calculations in our previous work [27]. The H_α line is used widely to calculate the electron density when the H_α line can be detected in the plasma, which has a higher precision as it is well isolated, it is strongly affected by the linear Stark effect and does not exhibit self-absorption [31, 32]. Experimentally, the H element is contributed by the oil film and exhibits sufficient reproducibility to be used for the calculation of the electron density. Multi-Saha–Boltzmann plots are used to deduce the temperature. A detailed description of the procedures used together with a list of the chosen lines can be found in our previous publication [27]. The relative standard deviations of the electron density and the temperature are calculated to be 20% for the Ar I line, 15% for the H_α line and 10%, respectively.

In Fig. 6, the axial extension of the electron density and the temperature for the uncoated aluminum substrate exhibits a similar trend to those in the results observed in our previous work although some experimental conditions have been changed, such as laser energy [27, 29]. The profiles of the electron density and the temperature show a plateau of slow variation in the middle of the distribution. They decrease near the target surface and in the periphery of the plasma due to the thermal conduction in the interfaces with the target and with the cold ambient gas, as shown in Fig. 6. However, for the plasma induced from the coated aluminum substrate, obvious differences in the electron density and temperature can be seen in Fig. 6. In Fig. 6(a), the axial profiles of the electron density for the coated aluminum substrate are narrower than that for the uncoated aluminum substrate, especially at a delay time of 0.5 μs, while the electron density and temperature are much higher at this delay. This means that the presence of the thin gel layer on the surface of the target does not reduce the density and temperature of the generated plasma. From the profiles of the electron density and temperature, we can see that at 0.5 μs, the plasma is still confined close to the target. This indicates that up to this time delay, the propagation of the plasma is efficiently slowed down due to the presence of the gel layer on the surface of the target. Such a constraint disappears between delays of 0.5 and 1.0 μs.

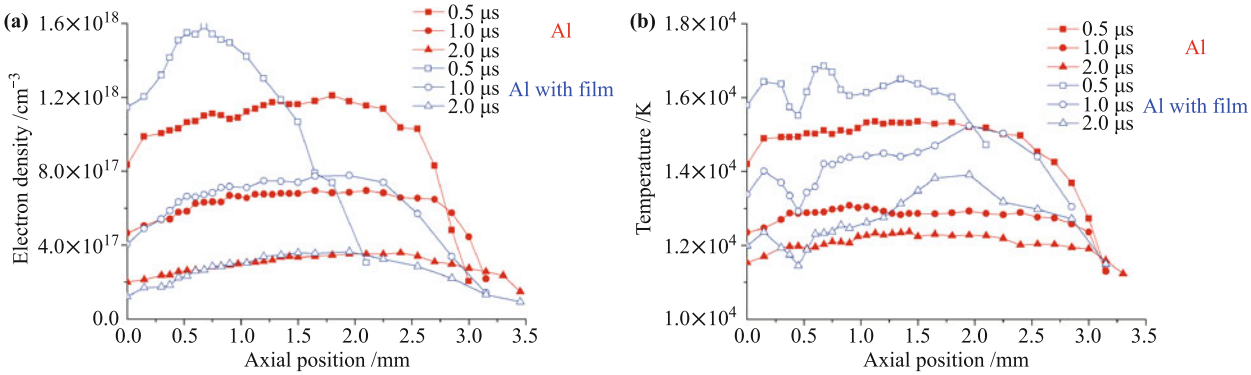

Fig. 6 Axial distribution of **(a)** the electron density and **(b)** the temperature of the plasma from the aluminum substrate with and without oil film in different delay times.

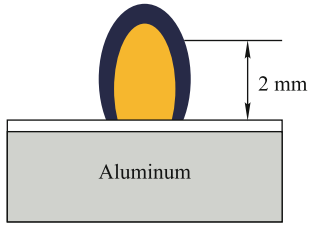

Fig. 7 The optimal emission zone of elements from the gel layer.

Moreover, for the electron density profile in Fig. 6(a), we note an accumulation of electrons around a height of 0.75 mm. Such an accumulation is consistent with the confinement of the aluminum plume at short delays due to the initial presence of the oil film on the surface of the target.

With the increasing delay, the electron density is almost in the same level as that for uncoated aluminum substrates, as shown in Fig. 6(a), although the temperature is still much higher, especially in the periphery of the plasma (about 2 mm away from the target surface). As shown in Fig. 6(b) the temperature is up 15 000 K in delay time 1.0 μs which is usually higher than that obtained in the plasma of solid and liquid samples under the same experimental conditions. This observation confirms the high temperature conditions necessary for the observation of a zone of emission from chlorine for a time delay larger than 1.0 μs around the front of the plasma, as shown in Fig. 3(d). These findings explain why we can observe the strongest emissions of elements from the oil film along the central axial profile in the periphery of the plasma. Figure 7 shows the optimal emission zone of elements from the gel layer. We remark that the strongest emissions of elements from the gel layer can be observed at 2 mm above the target after a detection delay of 1.0 μs.

4 Conclusion

In conclusion, the characteristics of the plasma induced from aluminum substrates with and without a coating of a thin layer oil film have been investigated. The Al emission induced by the uncoated aluminum substrates always extends near the target surface with increasing time delay, while the Al emission induced from the coated aluminum substrates extends away from the target surface to ablate the oil film and finally form a bifurcating circulation of aluminum vapor against a spherical confinement wall in front of the plume. Because of the confinement of the oil film, the plasma temperature remains high enough in the zone of 2 mm above the surface to excite the chlorine. Therefore, the strongest emissions of elements from the gel layer can be observed at 2 mm above the target after a detection delay of 1.0 μs. The high temperature reached in the plasma consisting of a mixture of substances from the target, the gel layer, and the ambient gas allows us to consider the application of the demonstrated ablation mechanism to the analysis of gel-like liquids or soft materials. It has also demonstrated the fact that it is feasible for indirect laser induced breakdown spectroscopy to detect trace elements sensitively through forming a transparent thin gel layer on the surface of a metallic aluminum substrate.

Acknowledgements The authors thank the French Rhone-Alps Region, the French Centre National de la Recherche Scientifique (CNRS) and the National Natural Science Foundation of China (NSFC) for their supports to the international collaboration and exchange programs. Two of the authors (J. S. Xiu and X. S. Bai) thank the China Scholarship Council (CSC) for their support.

References

1. Y. H. Wei, J. Y. Zhang, T. C. Dai, T. H. Tu, and L. G. Luo, Determination of chlorine in hogwash oil and edible oil by ion chromatograph, *Food Science* 32(12), 213 (2011)
2. Q. A. Ricardo, M. S. Roseli, C. C. Reinaldo, M. Norbert, and L. P. S. Carmem, The determination of trace in lubricating oils by atomic spectrometry, *Spectrochim. Acta B* 62(9), 952 (2007)
3. L. Caneve, F. Colao, F. Sarto, V. Spizzichino, and M. Vadrucci, Laser-induced breakdownspectroscopy as a diagnostic tool for thin films elemental composition, *Spectrochim. Acta B* 60(7–8), 1098 (2005)
4. P. Celio, C. Juliana, M. C. S. Lucas, and B. G. Fabinao, Laser induced breakdown spectroscopy, *J. Braz. Chem. Soc.* 18(3), 463 (2007)
5. A. De Giacomo, M. Dell'Aglio, O. De Pascale, and M. Capitelli, From single pulse to double pulse ns-Laser Induced Breakdown Spectroscopy under water: Elemental analysis of aqueous solutions and submerged solid samples, *Spectrochim. Acta B* 62(8), 721 (2007)
6. Z. Wang, T. B. Yuan, Z. Y. Hou, W. D. Zhou, J. D. Lu, H. B. Ding, and X. Y. Zeng, Laser-induced breakdown spectroscopy in China, *Front. Phys.* 9(4), 419 (2014)
7. J. Yu and R. E. Zheng, Laser-induced plasma and laser-induced breakdown spectroscopy (LIBS) in China: The challenge and the opportunity, *Front. Phys.* 7(6), 647 (2012)
8. F. Z. Dong, X. L. Chen, Q. Wang, L. X. Sun, H. B. Yu, Y. X. Liang, J. G. Wang, Z. B. Ni, Z. H. Du, Y. W. Ma, and J. D. Lu, Recent progress on the application of LIBS for metallurgical online analysis in China, *Front. Phys.* 7(6), 679 (2012)
9. L. Zhang, Z. Y. Hu, W. Y. Bao, D. Huang, W. G. Ma, L. Dong, H. P. Wu, Z. X. Li, L. T. Xiao, and S. T. Jia, Recent progress on laser-induced breakdown spectroscopy for the monitoring of coal quality and unburned carbon in fly

ash, *Front. Phys.* 7(6), 690 (2012)

10. V. S. Burakov, N. V. Tarasenko, M. I. Nedelko, V. N. Kononovb, N. N. Vasilevb, and S. N. Isakov, Analysis of lead and sulfur in environmental samples by double pulse laser induced breakdown spectroscopy, *Spectrochim. Acta B* 64(2), 141 (2009)
11. F. Boué-Bigne, Laser induced breakdown spectroscopy applications in the steel industry: Rapid analysis of segregation and decarburization, *Spectrochim. Acta B* 63 (10), 1122 (2008)
12. J. Kaiser, M. Galiová, K. Novotný, R. Èervenk, L. Reale, J. Novotný, M. Liška, O. Samek, V. Kanický, A. Hrdlièk, K. Stejskal, V. Adam, and R. Kizek, Mapping of lead, magnesium and copper accumulation in plant tissues by laser induced breakdown spectroscopy and laser ablation inductively coupled plasma mass spectrometry, *Spectrochim. Acta B* 64(1), 67 (2009)
13. P. Fichet, P. Mauchien, J. F. Wagner, and C. Moulin, Quantitative elemental determination inwater and oil by laser induced breakdown spectroscopy, *Anal. Chim. Acta* 429(2), 269 (2001)
14. M. A. Gondal and T. Hussain, Determination of poisonous metals in wastewater collected from paint manufacturing plant using laser-induced breakdown spectroscopy, *Talanta* 71(1), 73 (2007)
15. A. Kumar, F. Y. Yueh, and J. P. Singh, Double-pulse laser-induced breakdown spectroscopy with liquid jets of different thicknesses, *Appl. Opt.* 42(30), 6047 (2003)
16. N. K. Rai and A. K. Rai, LIBS-An efficient approach for the determination of Cr in industrial wastewater, *J. Hazard. Mater.* 150(3), 835 (2008)
17. R. L. VanderWal, T. M. Ticich, J. R. West, and Jr. P. A. Householder, Trace metal detection by Laser-Induced Breakdown Spectroscopy, *Appl. Spectrosc.* 53(10), 1226 (1999)
18. Z. J. Chen, H. K. Li, M. Liu, and R. H. Li, Fast and sensitive trace metal analysis in aqueous solutions by laser-induced breakdown spectroscopy using wood slice substrates, *Spectrochim. Acta B* 63(1), 64 (2008)
19. D. Alamelu, A. Sarkar, and S. K. Aggarwal, Laser-induced breakdown spectroscopy for simultaneous determination of Sm, Eu and Gd in aqueous solution, *Talanta* 77(1), 256 (2008)
20. Y. L. Yu, W. D. Zhou, H. G. Qian, X. J. Su, and K. Ren, Simultaneous determination of trace lead and chromium in water using laser-induced breakdown spectroscopy and paper substrate, *Plasma Sci. Technol.* 16(7), 683 (2014)
21. Q. Y. Lin, Z. M. Wei, M. J. Xu, S. Wang, G. H. Niu, K. P. Liu, Y. X. Duan, and J. Yang, Laser-induced breakdown spectroscopy for solution sample analysis using porous electrospun ultrafine fibers as a solid-phase support, *RSC Advances* 4(28), 14392 (2014)
22. A. Nadir, Ü. Y. Semira, A. A. Dilek, Y. Erife, Ultrasonic nebulization-sample introduction system for quantitative analysis of liquid samples by laser-induced breakdown spectroscopy, *Spectrochim. Acta B* 74–75(8–9), 87 (2012)
23. P. Yaroshchyk, R. J. S. Morrison, D. Body, and B. L. Chadwick, Quantitative determination of wear metal in engine oils using laser-induced breakdown spectroscopy: A comparison between liquid jets and static liquids, *Spectrochim. Acta B* 60(7–8), 986 (2005)
24. I. Y. Elnasharty, A. K. Kassem, M. Sabsabi, and M. A. Harith, Diagnosis of lubricating oil by evaluating cyanide and carbon molecular emission lines in laser induced breakdown spectra, *Spectrochim. Acta B* 66(8), 588 (2011)
25. M. A. Aguirre, S. Legnaioli, F. Almodóvar, M. Hidalgo, V. Palleschi, and A. Canals, Elemental analysis by surface-enhanced Laser-Induced Breakdown Spectroscopy combined with liquid-liquid microextraction, *Spectrochim. Acta B* 79–80(1–2), 88 (2013)
26. L. St-Onge, E. Kwong, M. Sabsabi, and E. B. Vadas, Quantitative analysis of pharmaceutical products by laser-induced breakdown spectroscopy, *Spectrochim. Acta B* 57(7), 1131 (2002)
27. X. S. Bai, Q. L. Ma, V. Motto-Ros, J. Yu, D. Sabourdy, L. Nguyen, and A. Jalocha, Convoluted effect of laser fluence and pulse duration on the property of a nanosecond laser-induced plasma into an argon ambient gas at the atmospheric pressure, *J. Appl. Phys.* 113(1), 013304 (2013)
28. A. Sáinz, A. Díaz, D. Casas, M. Pineda, F. Cubillo, and M. D. Calzada, Abel inversionapplied to a small set of emission data from a microwave plasma, *Appl. Spectrosc.* 60(3), 229 (2006)
29. Q. L. Ma, V. Motto-Ros, W. Q. Lei, M. Boueri, X. S. Bai, L. J. Zheng, H. P. Zeng, and J. Yu, Temporal and spatial dynamics of laser-induced aluminum plasma in argon background at atmospheric pressure: Interplay with the ambient gas, *Spectrochim. Acta B* 65(11), 89 (2010)
30. T. Sakka, T. Nakajima, and Y. H. Ogata, Spatial population distribution of laser ablationspecies determined by self-reversed emission line profile, *J. Appl. Phys.* 92(5), 2296 (2002)
31. A. M. El Sherbini, H. Hegazy, and Th. M. El Sherbini, Measurement of electron density utilizing the H_α-line from laser produced plasma in air, *Spectrochim. Acta B* 61(5), 532 (2006)
32. H. R. Griem, Spectral Line Broadening by Plasmas, New York: Academic Press, 1974